

Constantia Alexandrou

Parton distribution functions from Lattice QCD

Abstract We present recent results on the first moments of parton distributions using gauge configurations generated with two degenerate flavors of light twisted mass quarks with pion mass fixed approximately to its physical value. We also present a first study of the vector parton distribution function using a twisted mass ensemble at pion mass of 373 MeV.

Keywords 11.15.Ha, 12.38.Gc, 12.38.Aw

1 Introduction

Although nucleon structure has been an area of intensive activity within lattice QCD for a number of years, it is only recently that simulations with near physical parameters both in terms of the value of the pion mass (referred to as physical point), as well as, with respect to the lattice volume and lattice spacing have become available [1; 2; 3; 4; 5; 6; 7; 8; 9]. Generalized parton distributions (GPDs) encode information related to nucleon structure that complements the information extracted from form factors [10; 11; 12]. Their forward limit coincides with the usual parton distribution functions (PDFs) and, using Ji's sum rule [13], allows one to determine the contribution of a specific parton to the nucleon spin. In the context of the "proton spin puzzle", which refers to the unexpectedly small fraction of the total spin of the nucleon carried by quarks, this has triggered intense experimental activity [14; 15; 16; 17; 18]. Calculations using gauge configurations produced with physical values of the light quark mass, pose new challenges associated with the slower convergence of the inversion of the Dirac operator and the increase of gauge noise requiring very large computational resources. Therefore, techniques to speedup the inversions are critical in order to obtain results at the physical point. In Fig. 1 we show the speedup achieved when deflation of lowest eigen-modes is applied. The best improvement is achieved with exact deflation of the lowest about 1800 eigen-modes, which yields a speed-up of a factor of 20 as compared to the conjugate gradient method after about 1000 right hand sides (rhs) that is the typical number of rhs in our production runs.

2 Evaluation of matrix elements in lattice QCD

In Fig. 1 we show the contributions entering the evaluation of a hadron matrix element. One needs to compute the three-point function given by

Constantia Alexandrou
Department Physics, University of Cyprus, P.O. Box 20537, 1678 Nicosia, Cyprus, and
Computation-based Science and Technology Research Research, The Cyprus Institute, 20 Kavafi Str., Nicosia 2121, Cyprus
Tel.: +357-22-892829
E-mail: alexand@ucy.ac.cy

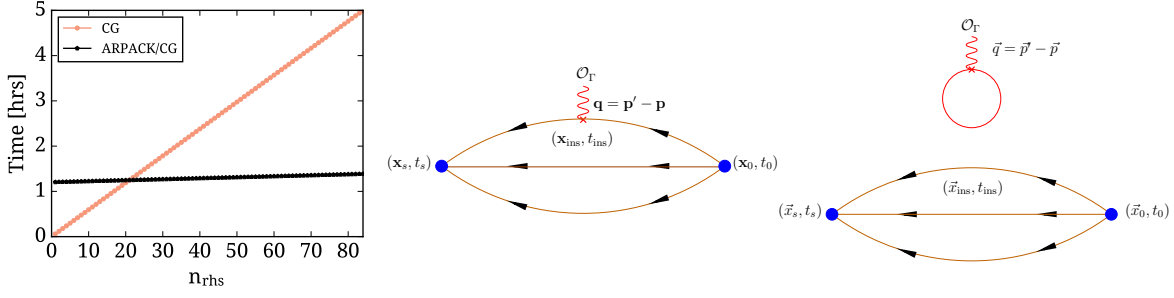


Fig. 1 Speedup achieved with exact deflation as a function of the number of rhs n_{rhs} (left). Connected (middle) and disconnected (right) contributions to a three-point function.

$$G^{\mu\nu}(\Gamma, \mathbf{q}, t_s, t_{\text{ins}}) = \sum_{\mathbf{x}_s, \mathbf{x}_{\text{ins}}} e^{i\mathbf{x}_{\text{ins}} \cdot \mathbf{q}} \Gamma_{\beta\alpha} \langle J_\alpha(\mathbf{x}_s, t_s) \mathcal{O}_\Gamma^{\mu\nu}(\mathbf{x}_{\text{ins}}, t_{\text{ins}}) \bar{J}_\beta(\mathbf{x}_0, t_0) \rangle \quad (1)$$

and then form a ratio by dividing the three-point function by an appropriate combination of two-point functions:

$$R(t_s, t_{\text{ins}}, t_0) \xrightarrow{(t_s - t_{\text{ins}})\Delta \gg 1, (t_{\text{ins}} - t_0)\Delta \gg 1} \mathcal{M} \left[1 + \dots e^{-\Delta(\mathbf{p})(t_{\text{ins}} - t_0)} + \dots e^{-\Delta(\mathbf{p}')(t_s - t_{\text{ins}})} \right]. \quad (2)$$

In Eq. 2 \mathcal{M} is the desired matrix element, t_s, t_{ins}, t_0 the sink, insertion and source time-slices and $\Delta(\mathbf{p})$ the energy gap with the first excited state. Summing over the current insertion time t_{ins} we obtain

$$\sum_{t_{\text{ins}}=t_0}^{t_s} R(t_s, t_{\text{ins}}, t_0) = \text{Const.} + \mathcal{M}[(t_s - t_0) + \mathcal{O}(e^{-\Delta(\mathbf{p})(t_s - t_0)}) + \mathcal{O}(e^{-\Delta(\mathbf{p}')(t_s - t_0)})]. \quad (3)$$

In the summed ratio, excited state contributions are suppressed by exponentials decaying with $t_s - t_0$, rather than $t_s - t_{\text{ins}}$ and/or $t_{\text{ins}} - t_0$. However, one needs to fit the slope rather than to a constant, which increases the statistical uncertainty in the extracted value of the desired matrix element.

In order to extract the physical value of the matrix element from the lattice results one needs to carry out the renormalization of the lattice matrix element by evaluating the renormalization function $Z(\mu, a)$. The renormalization functions are typically computed non-perturbatively. In this work we performed a perturbative subtraction of $\mathcal{O}(a^2)$ lattice artifacts, which in general leads to a better determination of the renormalization functions [19].

3 Generalized Parton Distributions

The standard procedure to study generalized parton distributions in lattice QCD is to use factorization of the light cone matrix element in terms of local operators. There are three types of GPDs involving the following operators: i) the vector operator $\mathcal{O}_{V_a}^{\mu_1 \dots \mu_n} = \bar{\psi}(x) \gamma^{\{\mu_1} i \overleftrightarrow{D}^{\mu_2} \dots i \overleftrightarrow{D}^{\mu_n\} \frac{\tau_a}{2}} \psi(x)$, ii) the axial-vector operator $\mathcal{O}_{A_a}^{\mu_1 \dots \mu_n} = \bar{\psi}(x) \gamma^{\{\mu_1} i \overleftrightarrow{D}^{\mu_2} \dots i \overleftrightarrow{D}^{\mu_n\} \gamma_5 \frac{\tau_a}{2}} \psi(x)$ and iii) the tensor operator $\mathcal{O}_{T_a}^{\mu_1 \dots \mu_n} = \bar{\psi}(x) \sigma^{\{\mu_1, \mu_2} i \overleftrightarrow{D}^{\mu_3} \dots i \overleftrightarrow{D}^{\mu_n\} \frac{\tau_a}{2}} \psi(x)$. In the special case when no derivatives are present then one obtains the nucleon form factors, while for $Q^2 = 0$ one has the parton distribution functions (PDFs). In this work, we limit ourselves to one-derivative operators determining the first moments of these PDFs.

Generalized form factor decomposition of the vector one-derivative operator yields

$$\langle N(p', s') | \mathcal{O}_{V_3}^{\mu\nu} | N(p, s) \rangle = \bar{u}_N(p', s') \left[A_{20}(q^2) \gamma^{\{\mu} P^{\nu\}} + B_{20}(q^2) \frac{i\sigma^{\{\mu\alpha} q_\alpha P^{\nu\}}}{2m} + C_{20}(q^2) \frac{q^{\{\mu} q^{\nu\}}}{m} \right] \frac{1}{2} u_N(p, s) \quad (4)$$

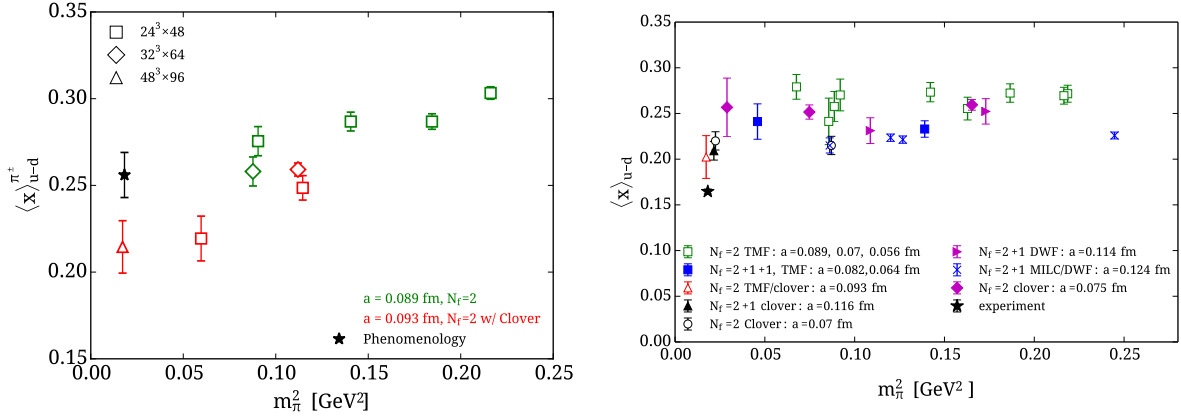


Fig. 2 $\langle x \rangle_{u-d}$ in the \overline{MS} scheme at $\mu = 2$ GeV for the pion (left) and for the nucleon (right). The experimental value for $\langle x \rangle_{u-d}$ shown here is from Ref. [20].

The nucleon spin due to a quark q is then determined by $J^q = \frac{1}{2} \left[A_{20}^q(0) + B_{20}^q(0) \right]$, while the momentum fraction is given by $\langle x \rangle_q = A_{20}^q(0)$.

3.1 Momentum fraction of the pion and the nucleon

In Fig. 2, we show results on the isovector $\langle x \rangle_{u-d}$ for which disconnected contributions are zero in the isospin limit for the pion and the nucleon in the \overline{MS} scheme at $\mu = 2$ GeV.

In the case of the pion we show results obtained using $N_f = 2$ twisted mass fermions. There is agreement between the clover-improved and non-clover improved ensembles [1] while no volume effects are observed within our statistical errors. The phenomenological value is extracted from a next-to-leading order analysis from Fermilab E-615 pionic Drell-Yan data [21]. The nucleon momentum fraction has been studied by a number of collaborations. In particular, near the physical point, in addition to $N_f = 2$ twisted mass plus clover-improved fermions from ETMC [1; 22; 23; 24; 23], there are results using $N_f = 2 + 1$ clover fermions with 2-HEX smearing from LHPC [9] and $N_f = 2$ clover fermions [25; 26] from QCDSF/UKQCD. As can be seen for the latest lattice results close to the physical pion mass, $\langle x \rangle_{u-d}$ approaches the physical value. Furthermore, these studies show that for bigger sink-source time separations the value decreases towards to the physical one. We note that, as the sink-source time separation increases, one needs increasingly larger statistics to attain statistical errors that can yield a meaningful result and this analysis is on-going.

3.2 Nucleon gluon moment

We consider the nucleon matrix element of the gluon operator $O_{\mu\nu} = -\text{Tr}[G_{\mu\rho}G_{\nu\rho}]$, where we take $\langle N | O_{44} - \frac{1}{3} O_{jj} | N \rangle$ at zero momentum, which yields directly $\langle x \rangle_g$. We use HYP-smearing to reduce noise and, for this operator, apply perturbative renormalization. We analyze two ensembles : one $N_f = 2 + 1 + 1$ twisted mass ensemble with $a = 0.082$ fm, $m_\pi = 373$ MeV, using 34,470 statistics and one $N_f = 2$ twisted mass plus clover ensemble, with $a = 0.093$ fm, $m_\pi = 132$ MeV and $\sim 155,800$ statistics. For the latter ensemble, we find $\langle x \rangle_g = 0.282(39)$ in \overline{MS} scheme at $\mu = 2$ GeV, which gives for the first time a determination of this important quantity at the physical value of the pion mass.

3.3 Nucleon spin

Having computed the generalized form factors A_{20} and B_{20} we can determine the nucleon spin carried by the quarks via the relation $J^q = \frac{1}{2} (A_{20}^q + B_{20}^q)$. The spin sum given by $\frac{1}{2} = \sum_q J^q = (\frac{1}{2} \Delta \Sigma^q + L^q) +$

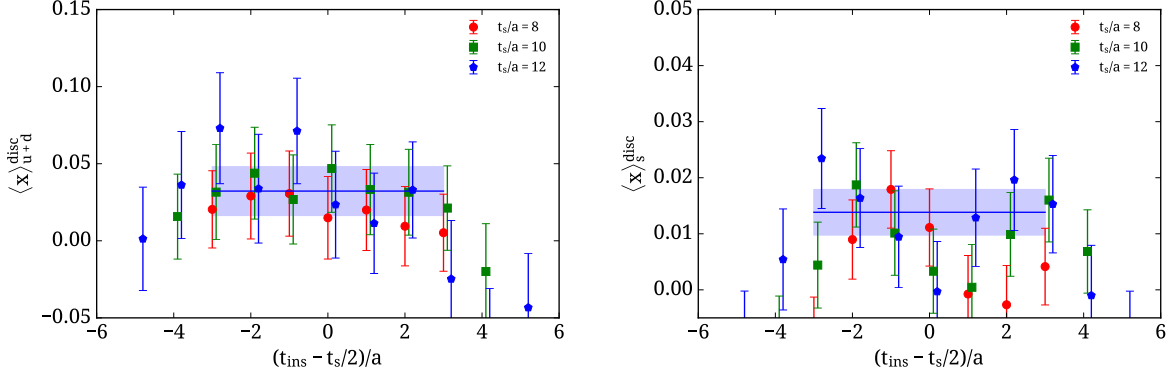


Fig. 3 Disconnected contributions to the nucleon momentum fraction at the physical point for the light (left) using currently 39000 measurements and for the strange (right) using about 185000 measurements.

J^G includes a gluon contribution J^G . The intrinsic quark spin is given by $\Delta\Sigma^q = g_A^q$, which has been computed within lattice QCD. Knowing J^q and g_A^q one can extract the angular momentum L^q .

In order to extract the individual quark contribution one needs to compute both the connected and disconnected parts shown schematically in Fig. 1. Connected contributions have been computed using the well established sequential inversion through the sink method. Disconnected contributions have been computed with new methods developed for graphics cards (GPUs). This was carried out for ensembles using $\mathcal{O}(150,000)$ statistics for the $N_f = 2 + 1 + 1$ ensemble of twisted mass fermions at $m_\pi = 373$ MeV [27] as well as using an $N_f = 2$ ensemble of twisted mass fermions with a clover term at $m_\pi = 132$ MeV [28], which is still on-going. We show in Fig. 3 the momentum fraction $\langle x \rangle_q = A_{20}^q(0)$ arising from the disconnected part. As can be seen, it is non-zero for both the light and the strange quarks. Whereas $A_{20}^q(0)$ is accessible directly at $Q^2 = 0$, $B_{20}(0)$ is not, requiring extrapolation to $Q^2 = 0$. Although we have computed the disconnected contributions to B_{20} for the few lowest Q^2 -values the results are consistent with zero and we will ignore them in what follows. The disconnected intrinsic spin $\Delta\Sigma^q$ is also found to be non-zero. We show in Fig. 4 the total spin J^q as well as $\Delta\Sigma^{u+d}$ at the physical point as well as $\Delta\Sigma^{u+d+s}$. As can be seen, including the disconnected contributions brings agreement with the experimental value in the case of $\Delta\Sigma$. Using $L^q = J^q - \frac{1}{2}\Delta\Sigma^q$ we obtain results on the angular momentum. The major outcome is that disconnected contributions produce a non-zero angular momentum at the physical point. At the physical point, our preliminary values are $J^{u+d} = 0.296(17)$ and $L^{u+d} = 0.067(28)$, while $\frac{1}{2}\Delta\Sigma^{u+d} = 0.229(20)$ and $\frac{1}{2}\Delta\Sigma^{u+d+s} = 0.211(21)$, where for the first time, disconnected contributions are included.

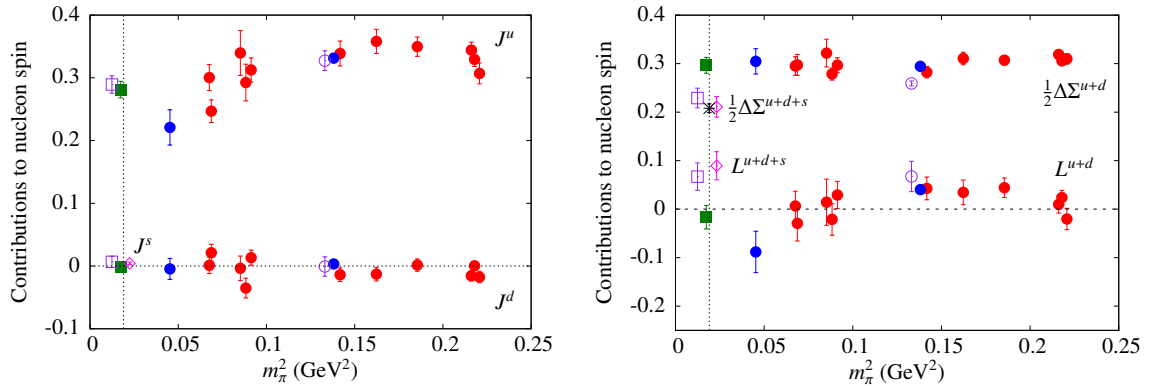


Fig. 4 The total quark spin (left) carried by the light and the strange quarks and $\Delta\Sigma^{u+d}$ and L^{u+d} (right) in the $\overline{\text{MS}}$ scheme at 2 GeV using $N_f = 2$ and $N_f = 2 + 1 + 1$ twisted mass fermions. Open circles and open squares include disconnected contributions from the u and d quarks, while the open diamonds also include the strange quark contribution. The asterisk is the experimental value of the intrinsic spin.

3.4 Direct evaluation of parton distribution functions - an exploratory study

We consider the matrix element: $\tilde{q}(x, \Lambda, P_3) = \int_{-\infty}^{+\infty} \frac{dz}{4\pi} e^{-izxP_3} \langle P | \bar{\psi}(z, 0) \gamma_3 W(z) \psi(0, 0) | P \rangle_{h(P_3, z)}$ where $\tilde{q}(x)$ is the quasi-distribution defined in Ref. [29], which can be computed in lattice QCD. First results are obtained for $N_f = 2 + 1 + 1$ clover fermions on HISQ sea [30] and for an $N_f = 2 + 1 + 1$ TMF ensemble with $m_\pi = 373$ MeV [31] for which we show results in Fig. 5 on the isovector distribution $q^{u-d}(x)$ for 5 steps of HYP smearing. The matching to the PDF $q(x)$ is done using

$$q(x, \mu) = \tilde{q}(x, \Lambda, P_3) - \frac{\alpha_s}{2\pi} \tilde{q}(x, \Lambda, P_3) \delta Z_F^{(1)} \left(\frac{\mu}{P_3}, \frac{\Lambda}{P_3} \right) - \frac{\alpha_s}{2\pi} \int_{-1}^1 \frac{dy}{y} Z^{(1)} \left(\frac{x}{y}, \frac{\mu}{P_3}, \frac{\Lambda}{P_3} \right) \tilde{q}(y, \Lambda, P_3) + \mathcal{O}(\alpha_s^2) \quad (5)$$

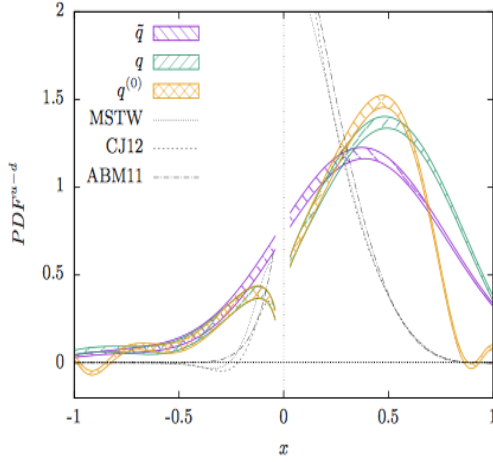


Fig. 5 Results on the unrenormalized $q(x)$ for 5-HYP steps, $P_3 = 4\pi/L$ from Ref. [31].

We note that: i) The calculation of the leading UV divergences in \tilde{q} perturbatively is done keeping P_3 fixed while taking $\Lambda \rightarrow \infty$ (in contrast to first taking $P_3 \rightarrow \infty$ for the renormalization of q); ii) The renormalization procedure is still under study and thus here we identify the UV regulator as μ for $q(x)$ and as Λ for the case of the quasi-distribution $\tilde{q}(x)$. The dependence on the UV regulator Λ will be translated, in the end, into a renormalization scale μ after proper renormalization; iii) Single pole terms cancel when combining the vertex and wave function corrections, and double poles are reduced to a single pole that are taken care via the principal value prescription; iv) A divergent term remains in $\delta Z^{(1)}$ that depends on the cut-off x_c

4 Conclusions

Simulations at near physical parameters of QCD are yielding important results on the structure of hadrons. In this work we have shown results on nucleon observables taking into account for the first time disconnected contributions at the physical point, which are shown to be crucial to obtain agreement with experiment for the intrinsic spin of the nucleon. Exploration of new techniques to compute hadron PDFs, charge radii and electric dipole moments is on-going, as well as, the development of techniques for resonances and for *ab Initio* Nuclear Physics [32]. This thus represents a very rich program for zero-temperature hadron and nuclear physics and we expect rapid progress in many of these areas in the near future.

Acknowledgements I would like to thank all members of the ETM Collaboration for a most enjoyable collaboration and in particular A. Abdel-Rehim, M. Constantinou, K. Jansen, K. Hadjiyiannakou, Ch. Kallidonis, G. Koutsou, B. Kostrzewa, F. Steffens, C. Urbach, C. Wiese and A. Vaquero for their invaluable contributions to the results presented here. This work was supported by a grant from the Swiss National Supercomputing Centre (CSCS) under project ID s540 and in addition used computational resources from the John von Neumann-Institute for Computing on the Juropa system and the BlueGene/Q system Juqueen at the research center in Jülich, resources from the Gauss Centre for Superccomputing on HazelHen (HLRS) and PRACE project access to the Tier-0 computing resources Curie (CEA), Fermi (CINECA) and SuperMUC (LRZ).

References

1. A. Abdel-Rehim et al. Nucleon and pion structure with lattice QCD simulations at physical value of the pion mass. *Phys. Rev.*, D92(11):114513, 2015.

2. A. Abdel-Rehim et al. Simulating QCD at the Physical Point with $N_f = 2$ Wilson Twisted Mass Fermions at Maximal Twist. *arXiv:1507.05068*, 2015.
3. Gunnar Bali, Sara Collins, Meinulf Gockeler, Rudolf Rdl, Andreas Schfer, and Andre Sternbeck. Nucleon generalized form factors from lattice QCD with nearly physical quark masses. *arXiv:1601.04818*, 2016.
4. Tanmoy Bhattacharya, Vincenzo Cirigliano, Saul Cohen, Rajan Gupta, Anosh Joseph, Huey-Wen Lin, and Boram Yoon. Iso-vector and Iso-scalar Tensor Charges of the Nucleon from Lattice QCD. *Phys. Rev.*, D92(9):094511, 2015.
5. S. Durr et al. Lattice computation of the nucleon scalar quark contents at the physical point. *arXiv:1510.08013*, 2015.
6. Shigemi Ohta. Systematics analyses on nucleon isovector observables in 2+1-flavor dynamical domain-wall lattice QCD near physical mass. *PoS, LATTICE2014*:149, 2014.
7. J. R. Green, J. W. Negele, A. V. Pochinsky, S. N. Syritsyn, M. Engelhardt, and S. Krieg. Nucleon electromagnetic form factors from lattice QCD using a nearly physical pion mass. *Phys. Rev.*, D90:074507, 2014.
8. R. Horsley, Y. Nakamura, A. Nobile, P.E.L. Rakow, G. Schierholz, et al. Nucleon axial charge and pion decay constant from two-flavor lattice QCD. *arXiv:1302.2233*, 2013.
9. J.R. Green, M. Engelhardt, S. Krieg, J.W. Negele, A.V. Pochinsky, et al. Nucleon Structure from Lattice QCD Using a Nearly Physical Pion Mass. *arXiv:1209.1687*, 2012.
10. Dieter Mueller, D. Robaschik, B. Geyer, F.M. Dittes, and J. Horejsi. Wave functions, evolution equations and evolution kernels from light ray operators of QCD. *Fortsch.Phys.*, 42:101, 1994.
11. Xiang-Dong Ji. Deeply virtual Compton scattering. *Phys.Rev.*, D55:7114–7125, 1997.
12. A.V. Radyushkin. Nonforward parton distributions. *Phys.Rev.*, D56:5524–5557, 1997.
13. Xiang-Dong Ji. Gauge invariant decomposition of nucleon spin and its spin - off. *Phys.Rev.Lett.*, 78:610–613, 1997.
14. A. Airapetian et al. Separation of contributions from deeply virtual Compton scattering and its interference with the Bethe-Heitler process in measurements on a hydrogen target. *JHEP*, 0911:083, 2009.
15. S. Chekanov et al. A Measurement of the Q^2 , W and t dependences of deeply virtual Compton scattering at HERA. *JHEP*, 0905:108, 2009.
16. F.D. Aaron et al. Measurement of deeply virtual Compton scattering and its t -dependence at HERA. *Phys.Lett.*, B659:796–806, 2008.
17. C. Munoz Camacho et al. Scaling tests of the cross-section for deeply virtual compton scattering. *Phys.Rev.Lett.*, 97:262002, 2006.
18. S. Stepanyan et al. First observation of exclusive deeply virtual Compton scattering in polarized electron beam asymmetry measurements. *Phys.Rev.Lett.*, 87:182002, 2001.
19. C. Alexandrou, M. Constantinou, T. Korzec, H. Panagopoulos, and F. Stylianou. Renormalization constants of local operators for Wilson type improved fermions. *Phys.Rev.*, D86:014505, 2012.
20. S. Alekhin, J. Blumlein, and S. Moch. Parton Distribution Functions and Benchmark Cross Sections at NNLO. *Phys. Rev.*, D86:054009, 2012.
21. K. Wijesooriya, P.E. Reimer, and R.J. Holt. The pion parton distribution function in the valence region. *Phys.Rev.*, C72:065203, 2005.
22. A. Abdel-Rehim, C. Alexandrou, P. Dimopoulos, R. Frezzotti, K. Jansen, et al. Progress in Simulations with Twisted Mass Fermions at the Physical Point. *PoS, LATTICE2014*:119, 2014.
23. A. Abdel-Rehim, Ph. Boucaud, N. Carrasco, A. Deuzeman, P. Dimopoulos, et al. A first look at maximally twisted mass lattice QCD calculations at the physical point. *PoS, LATTICE2013*:264, 2013.
24. Abdou Abdel-Rehim, Florian Burger, Alber Deuzeman, Karl Jansen, Bartosz Kostrzewa, Luigi Scorzato, and Carsten Urbach. Recent developments in the tmLQCD software suite. *PoS, LATTICE2013*:414, 2014.
25. Gunnar S. Bali, Sara Collins, Benjamin Gille, Meinulf Gckeler, Johannes Najjar, Rudolf H. Rdl, Andreas Schfer, Rainer W. Schiel, Andr Sternbeck, and Wolfgang Sldner. The moment $\langle x \rangle_{u-d}$ of the nucleon from $N_f = 2$ lattice QCD down to nearly physical quark masses. *Phys. Rev.*, D90(7):074510, 2014.
26. D. Pleiter et al. Nucleon form factors and structure functions from $N(f)=2$ Clover fermions. *PoS, LATTICE2010*:153, 2010.
27. A. Abdel-Rehim, C. Alexandrou, M. Constantinou, V. Drach, K. Hadjiyiannakou, K. Jansen, G. Koutsou, and A. Vaquero. Disconnected quark loop contributions to nucleon observables in lattice QCD. *Phys. Rev.*, D89(3):034501, 2014.
28. Abdou Abdel-Rehim, Constantia Alexandrou, Martha Constantinou, Kyriakos Hadjiyiannakou, Karl Jansen, Christos Kallidonis, Giannis Koutsou, and Alejandro Vaquero Avils-Casco. Disconnected quark loop contributions to nucleon observables using $N_f = 2$ twisted clover fermions at the physical value of the light quark mass. In *Proceedings, 33rd International Symposium on Lattice Field Theory (Lattice 2015)*, 2015.
29. Xiangdong Ji. Parton Physics on a Euclidean Lattice. *Phys. Rev. Lett.*, 110:262002, 2013.
30. Huey-Wen Lin, Jiunn-Wei Chen, Saul D. Cohen, and Xiangdong Ji. Flavor Structure of the Nucleon Sea from Lattice QCD. *Phys. Rev.*, D91:054510, 2015.
31. Constantia Alexandrou, Krzysztof Cichy, Vincent Drach, Elena Garcia-Ramos, Kyriakos Hadjiyiannakou, Karl Jansen, Fernanda Steffens, and Christian Wiese. Lattice calculation of parton distributions. *Phys. Rev.*, D92:014502, 2015.
32. Martin J. Savage. Nuclear Physics from Lattice Quantum Chromodynamics. In *12th Conference on the Intersections of Particle and Nuclear Physics (CIPANP 2015) Vail, Colorado, USA, May 19-24, 2015*, 2015.